THE JOURNAL OF PHYSICAL CHEMISTRY B

Article

pubs.acs.org/JPCB

Excited States Energies and Dynamics of Peridinin Analogues and the Nature of the Intramolecular Charge Transfer State in Carbonyl-Containing Carotenoids

Dariusz M. Niedzwiedzki,*[,†] Takayuki Kajikawa,[‡] Kazuyoshi Aoki,[‡] Shigeo Katsumura,[‡] and Harry A. Frank*[,§]

[†]Photosynthetic Antenna Research Center, Washington University in St Louis, Saint Louis, Missouri 63130, United States

[‡]Department of Chemistry, Kwansei Gakuin University, 669-1337, Hyogo, Japan

[§]Department of Chemistry, University of Connecticut, U-3060, 55 North Eagleville Road, Storrs, Connecticut 06269-3060, United States

Supporting Information

ABSTRACT: The lifetime of the lowest excited singlet state of carbonyl-containing carotenoids typically depends on the polarity of the solvent, an effect that has been attributed to the presence of an intramolecular charge transfer (ICT) state. The nature of this ICT state has yet to be clarified. In the present work, steady-state and ultrafast time-resolved optical spectroscopic experiments have been performed on peridinin and three synthetic analogues, C_{33}-peridinin, C_{35}-peridinin, and C_{39}-peridinin, which have different extents of π-electron conjugation. Steady-state absorption at cryogenic temperatures revealed new absorption bands on the long-wavelength side of the strongly allowed S_0 ($1^1A_g^-$) → S_2 ($1^1B_u^+$) transition that can be assigned to S_0 ($1^1A_g^-$) → S_1 ($2^1A_g^-$) absorption. Analysis of the time-resolved absorption and fluorescence data sets revealed that the influence of polarity of the solvent on the excited state lifetime is unique for each molecule, leading to subtle differences in the values in highly polar solvents. Measurements in the most polar solvent, acetonitrile, demonstrated that the ICT state lifetime is shortest at 6.4 ps for C_{39}-peridinin and gradually increases as the extent of π-electron conjugation decreases, becoming 10.6 ps for C_{33}-peridinin. This suggests that the energy of the ICT state is dependent on the number of conjugated carbon−carbon double bonds.

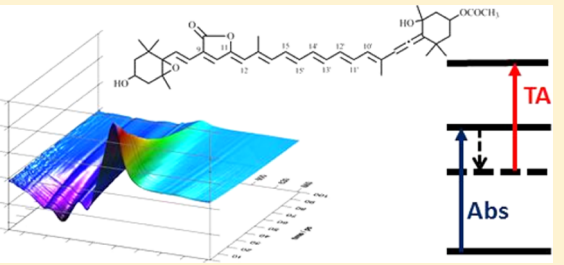

INTRODUCTION

Carotenoids are a class of photosynthetic pigments that occur naturally in higher plants, algae, and bacteria.[1,2] Most carotenoids have yellow, orange, or red coloration due to absorption in the visible wavelength region between 400 and 550 nm in which the strongly allowed S_0 ($1^1A_g^-$) → S_2 ($1^1B_u^+$) electronic transition occurs. Transitions to and from the ground state, S_0 ($1^1A_g^-$), and the lowest-lying excited state, S_1 ($2^1A_g^-$), are forbidden because one-photon processes require a change in symmetry (g ↔ u) and pseudoparity (+ ↔ −).[3] In addition, because of its negligible transition dipole moment, the S_1 ($2^1A_g^-$) state is not typically affected by changes in solvent environment. Therefore, for many carotenoids, the S_1 ($2^1A_g^-$) state lifetime remains constant, regardless of polarity and polarizability of the solvating medium.

The introduction of a carbonyl functional group into the conjugated π-electron system of double bonds in a carotenoid structure can induce a profound effect of solvent polarity on the lifetime of the S_1 ($2^1A_g^-$) excited singlet state. This effect has been reported for a number of ketolated carotenoids and carbonyl-containing model polyenes and has been explained by the presence of an intramolecular charge transfer state (ICT) coupled to the S_1 ($2^1A_g^-$) state.[4−11] The dependence of the S_1 ($2^1A_g^-$) state lifetime on solvent polarity has been rationalized by assuming that an increase in solvent polarity stabilizes the ICT state relative to the S_1 ($2^1A_g^-$) state, thereby leading to an increase in the rate constant for deactivation back to the ground S_0 ($1^1A_g^-$) state.[5,11] Although this model can account qualitatively for the experimental observations, the precise nature of the ICT state and its coupling to the S_1 ($2^1A_g^-$) state remain unclear.

Peridinin is exemplary as a carbonyl-carotenoid, exhibiting a large effect of solvent polarity on its S_1 ($2^1A_g^-$) state lifetime. The S_1 ($2^1A_g^-$) state of peridinin has a lifetime of ∼160 ps in the nonpolar solvent *n*-hexane. When peridinin is dissolved in the polar solvent methanol, the lifetime is dramatically reduced by more than an order of magnitude to ∼10 ps.[4,10,12−14] Peridinin is unusual structurally in that it is based on a C_{37} carbon skeleton instead of a typical C_{40} structure possessed by most carotenoids. It is also highly substituted and has a variety of functional groups, including an allene group and a lactone

Received: January 2, 2013
Revised: May 16, 2013

   dx.doi.org/10.1021/jp400038k | J. Phys. Chem. B XXXX, XXX, XXX−XXX

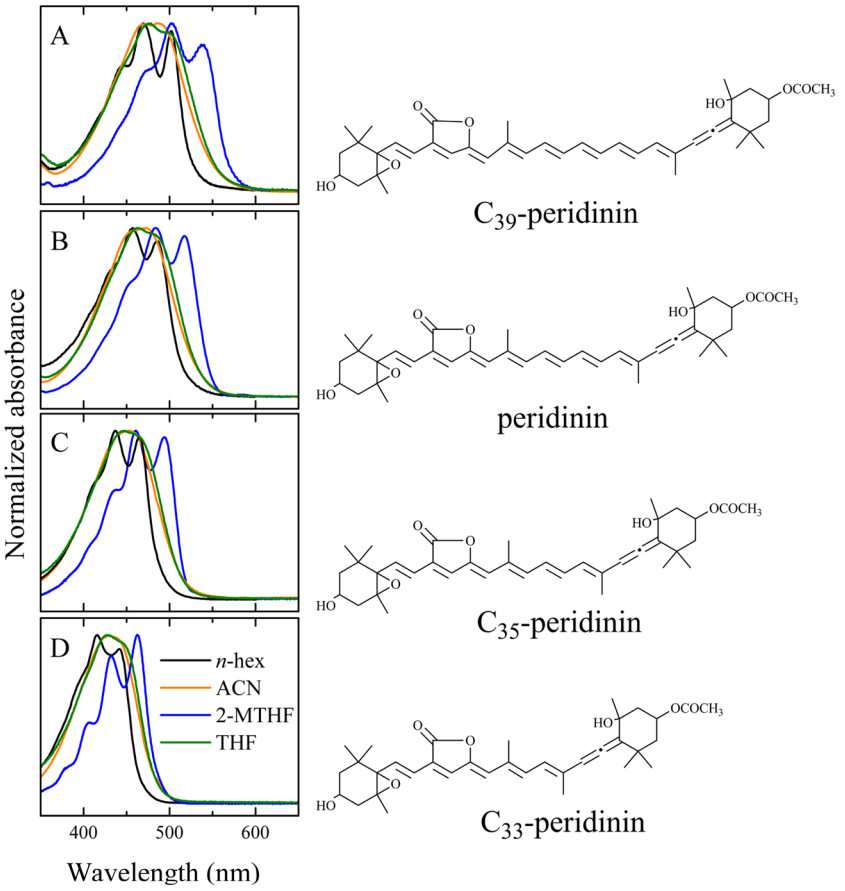

Figure 1. Steady-state absorption spectra and the molecular structures of (A) C_{39}-peridinin, (B) peridinin, (C) C_{35}-peridinin, and (D) C_{33}-peridinin. The spectra were measured at RT in *n*-hexane (*n*-hex), acetonitrile (ACN), and tetrahydrofuran (THF) and at 77 K in 2-methyltetrahydrofuran (2-MTHF).

ring with a keto group in conjugation with the π-electron system of carbon−carbon double bonds (Figure 1).

Ultrafast time-resolved optical spectroscopic studies carried out on a series of carbonyl-containing carotenoids having different extents of π-electron conjugation revealed that the effect of solvent becomes more pronounced for molecules with shorter conjugated systems of π-electron double bonds.[6−10] These reports have spawned various models for the nature of the ICT state, including the ICT state, as either uncoupled from S_1 ($2^1A_g^-$),[4,15] coupled to S_1 ($2^1A_g^-$) but being a distinct state,[16−18] quantum mechanically mixed with S_1 ($2^1A_g^-$),[13,19] or S_1 ($2^1A_g^-$) itself possessing a large intrinsic dipole moment due to coupling with the S_2 ($1^1B_u^+$) state.[20]

Recently, we reported the results of comparative steady-state and ultrafast time-resolved spectroscopic studies on peridinin and three synthetic analogues having different numbers of conjugated carbon−carbon double bonds, *N*, ranging from 6 to 9 (Figure 1). The analogues were denoted C_{33}-, C_{35}-, and C_{39}-peridinin. In all other ways, these molecules are structurally identical to peridinin. Time-resolved absorption spectroscopy performed in the visible range revealed that the effect of solvent polarity on the excited state spectra and dynamics depended on the extent of π-electron conjugation and became more pronounced as *N* decreased. In addition, the lifetime of the S_1 ($2^1A_g^-$) state, and presumably also the ICT state, of peridinin and all of the analogues was reported to converge to essentially the same value of ∼10 ps in the polar solvent, methanol.[14]

The present work extends this previous work and reports a time-resolved absorption and fluorescence spectroscopic investigation of peridinin and the C_{33}-, C_{35}-, and C_{39}-peridinin analogues in *n*-hexane, tetrahydrofuran, and acetonitrile, which have very different polarities but similar polarizabilities at RT. The spectroscopic studies presented here were extended into NIR, spanning the range from 400 to 1600 nm. In addition, we carried out measurements at 77 K on the molecules dissolved in 2-methyltetrahydrofuran. All of the time-resolved spectroscopic data were analyzed using global fitting methods. The data and analyses reveal more precise lifetimes and energies of the S_1 ($2^1A_g^-$) state than previously reported, demonstrate trends in stimulated emission from the ICT state, and help elucidate further the nature of the ICT state and its coupling to S_1 ($2^1A_g^-$). In addition, the extended delay times used for the transient absorption measurements (out to 8 ns compared to 1.6 ns from previous measurements) revealed that the peridinin analogues spontaneously form triplet states with yields that are strongly dependent on the π-electron conjugation length of the molecule.

MATERIALS AND METHODS

Synthesis and Purification of Peridinin Analogues. Peridinin was obtained from *Symbiodinium* cells. The cells were harvested and pelleted by centrifugation and then were dissolved in technical grade methanol to extract the pigments. The pigment extract was filtered and injected into an HPLC system employing a Zorbax Eclipse XDB-C18 reversed phase

dx.doi.org/10.1021/jp400038k | J. Phys. Chem. B XXXX, XXX, XXX−XXX

column (Agilent) (250 mm × 4.6 mm) using an isocratic flow rate of 1 mL/min and acetonitrile as a mobile phase. The synthesis of the C_{33}-, C_{35}-, and C_{39}-peridinin analogues has been described in detail previously.[21] Before carrying out the spectroscopic measurements, the molecules were dissolved in spectroscopic grade solvents with increasing polarity, $P(\varepsilon) = (\varepsilon - 1)/(\varepsilon + 2)$, but with similar polarizability (Lorentz−Lorenz equation), $R(n) = (n^2 - 1)/(n^2 + 2)$ for the experiments at RT (RT): *n*-hexane (*n*-hex, $P(\varepsilon) = 0.229$, $R(n) = 0.228$), tetrahydrofuran (THF, $P(\varepsilon) = 0.687$, $R(n) = 0.245$), acetonitrile (ACN, $P(\varepsilon) = 0.921$, $R(n) = 0.213$). For the cryogenic measurements, 2-methyltetrahydrofuran (2-MTHF) was used. Steady-state absorption spectra were recorded using a Perkin-Elmer Lambda 950 UV/vis/NIR spectrophotometer. All spectroscopic measurements at 77 K were performed using an Oxford OptistatDN liquid nitrogen cryostat.

Femtosecond Time-Resolved Transient Absorption Spectroscopy. Time-resolved pump−probe absorption experiments were carried out using Helios, a femtosecond transient absorption (TA) spectrometer (Ultrafast Systems, LCC) coupled to a femtosecond laser system based on Spectra-Physics components and described in detail previously.[22] The energy of the pump beam was set to 1 μJ/pulse in a spot size of 1 mm diameter corresponding to an intensity between 2.8 and 3.5×10^{14} photons/cm^2 per pulse depending on the excitation wavelength. The samples were excited at wavelengths coinciding with the 0−0 vibronic bands of the S_0 ($1^1A_g^-$) → S_2 ($1^1B_u^+$) transition. The optical densities (OD) of the samples were adjusted to 1−3 and then transferred to 2 mm path length cuvettes. During the measurements at RT, the samples were mixed continuously using a magnetic microstirrer to prevent photodegradation.

Time-Resolved Fluorescence Spectroscopy. Time-resolved fluorescence (TRF) experiments were carried out using a universal streak camera C5680 from Hamamatsu consisting of a cooled N51716-04 streak tube, a digital CCD camera (Orca2), a synchroscan unit M5675, a synchronous delay generator C6878, and an A6365-01 spectrograph from Bruker. Excitation pulses were generated by an ultrafast optical parametric oscillator (OPO) Inspire100 from Radiantis-Spectra-Physics pumped using a Mai-Tai ultrafast Ti:Sapphire laser generating ∼90 fs laser pulses at 820 nm with a frequency of 80 MHz. The excitation beam energy was kept between 20 and 100 mW and was focused on the sample in a circular spot of 2 mm diameter, which corresponds to a photon intensity of ∼0.8−4 × 10^{10} photons/cm^2 per pulse. Fluorescence was measured at a right angle orientation on samples having an OD of ∼0.5 at the maximum of their absorption band in a 1 cm square cuvette. To minimize reabsorption of emitted photons, the excitation beam spot was focused at a distance of ∼2 mm from the side of the cuvette that was aligned with the emission detector.

Transient Absorption Data Analysis and Global Fitting. Group velocity dispersion of the TA spectra was corrected using Surface Explorer (v.1.1) software from Ultrafast Systems LCC by building a dispersion correction curve from a set of initial times of transient signals obtained from single wavelength fits of the representative kinetics. Global fitting analysis was performed using a modified version of ASUfit, a program provided by Dr. Evaldas Katilius at Arizona State University (http://www.public.asu.edu/∼laserweb/asufit/asufit.html). The full width at half-maximum of instrument response function was obtained as one of the global fitting parameters and ranged between 100 and 200 fs for TA and up to 50 ps for TRF (depending from the temporal window of streak camera). For global fitting of TA data sets, an unbranched, unidirectional decay path model (A → B → C → D → ...) was used for fitting purposes. This model assumes that the energy losses are large enough that the reverse reaction rates are negligible. For global fitting of the TRF data sets, a simultaneous decay path model was used (sum of simultaneously and monoexponentially decaying molecular species). The spectral profiles obtained from sequential decay fitting of the TA data sets are termed evolution associated difference spectra (EADS); obtained from parallel decay fitting of the TRF data sets are termed decay associated spectra (DAS).[23]

RESULTS

Steady-State Absorption. The steady-state absorption spectra of peridinin and analogues taken at RT in *n*-hex, THF, and ACN and at 77 K in 2-MTHF are shown in Figure 1. Upon increasing the solvent polarity, the spectra broaden as is typical for carotenoids having a carbonyl group directly attached to the π-electron conjugation.[4] The spectral broadening can be attributed to a solvent polarity-induced increase in the number of conformational isomers, each of which exhibit slightly different spectra, which when summed together produce a broad, almost featureless, absorption band.[12] The spectral broadening effect is not the same for all of the peridinin analogues. It is more pronounced at RT for the molecules having shorter conjugated π-electron systems of double bonds.

Upon lowering the temperature to 77 K, the absorption spectra shift to longer wavelength by ∼20 nm. In addition, an enhancement in spectral resolution of the vibronic bands is induced. Interestingly, the 77 K absorption spectrum of C_{33}-peridinin differs from those of the other analogues in that the amplitude of its spectral origin (0−0) vibronic band is greatly enhanced. This suggest that there is a smaller horizontal displacement of the S_0 ($1^1A_g^-$) and S_2 ($1^1B_u^+$) potential energy surfaces compared with the other molecules.

In addition, a spectral shift of the ground state absorption upon lowering the temperature is expected and can be attributed to the significant increase in the refractive index of the 2-MTHF glass upon freezing. Comparative studies of the position of the steady-state absorption of peridinin in various aprotic polar solvents having different polarizabilities demonstrated that the position of the absorption spectrum is a linear function of polarizability of the solvent if the condition $\sim P(\varepsilon) - R(n) < 0.6$ is met. If $P(\varepsilon) - R(n) > 0.6$ (e.g. for ACN and acetone), a spectral shift is essentially absent.[4] A higher polarizability of the environment stabilizes the S_2 ($1^1B_u^+$) state and lowers the energy of the S_0 ($1^1A_g^-$) → S_2 ($1^1B_u^+$) transition. Richert[24] demonstrated that the ε value of 2-MTHF is functionally dependent on temperature and at 77 K has value ∼19 and $P(\varepsilon) \sim 0.86$. The refractive index of 2-MTHF at 77 K was determined to be ∼1.8,[25] which leads to an $R(n) = 0.43$, and $P(\varepsilon) - R(-) = 0.43$. Thus, the observed spectral shift for the analogues can be attributed to a simple change of the polarizability of 2-MTHF, even for such a high polarity glass. The observed enhancement in the resolution in the vibronic structure of the spectra (Figure 1), which is typically associated with the decrease in the conformational disorder of the frozen molecules, is very likely diminished due to a competing effect from environment polarity discussed earlier. Indeed, the enhancement of the vibronic structure of the absorption spectrum at low temperature is much smaller than usually

dx.doi.org/10.1021/jp400038k | J. Phys. Chem. B XXXX, XXX, XXX−XXX

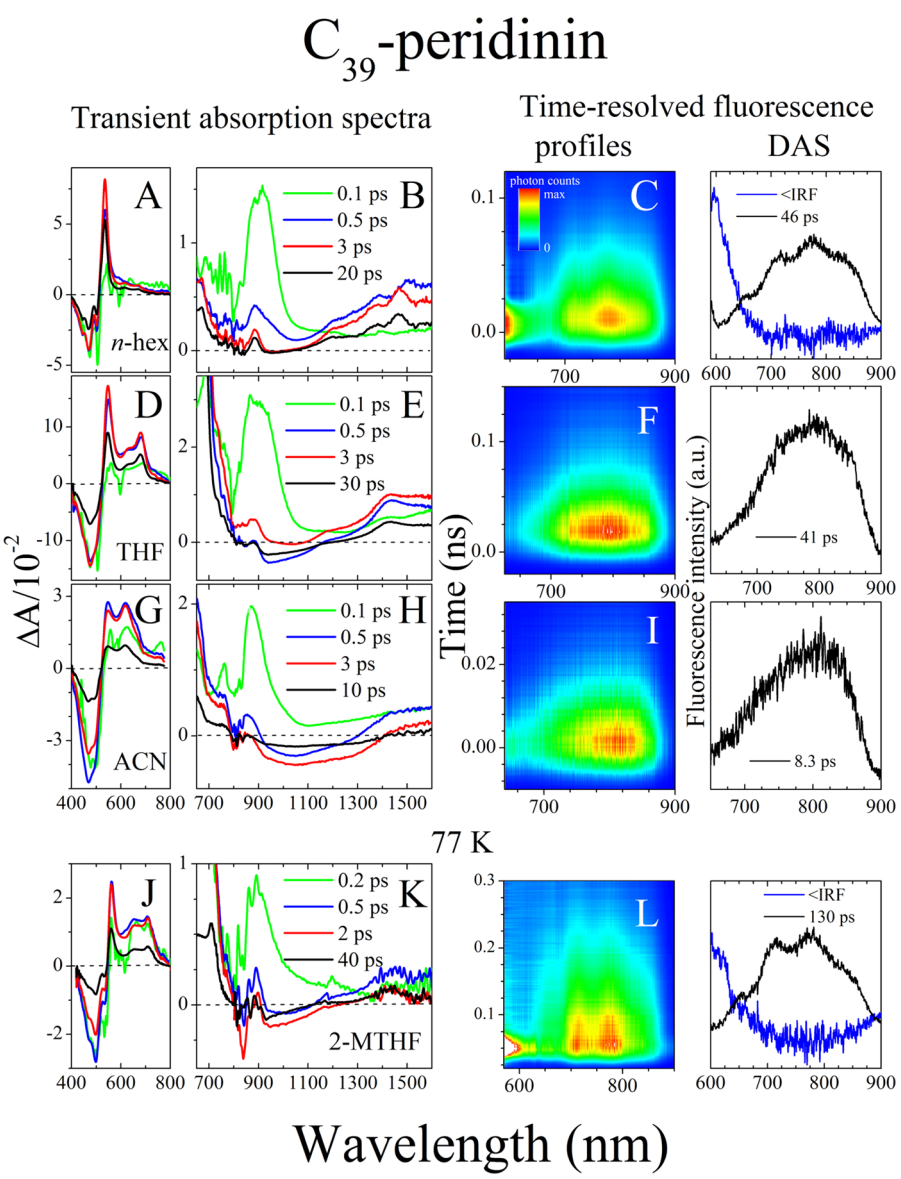

Figure 2. Transient absorption spectra, TRF contours and DAS profiles of C_{39}-peridinin. The measurements were carried out in *n*-hexane (*n*-hex), tetrahydrofuran (THF), and acetonitrile (ACN) at RT and in 2-methyltetrahydrofuran (2-MTHF) at 77 K. The long-lived DAS profiles may be assumed to be equal to the steady-state S_1 ($2^1A_g^-$) → S_0 ($2^1A_g^-$) fluorescence spectra. The lifetimes of the fluorescence decay are also provided. In the cases of *n*-hex and 2-MTHF, an additional short-lived DAS (shorter than instrument response function (IRF)) was necessary to obtain a satisfactory global fit. It represents fluorescence from the S_2 ($1^1B_u^+$) state (long wavelength tail). The samples were excited at 502 (*n*-hex), 500 (THF), 490 (ACN), and 540 nm (2-MTHF).

reported for carotenoids lacking carbonyl groups conjugated with the π-electron polyene chain.

Time-Resolved Absorption and Fluorescence. The TA spectra, TRF profiles, and the DAS profiles (obtained from global fitting of the TRF data sets) of C_{39}-peridinin taken upon excitation into the S_2 ($1^1B_u^+$) state are shown in Figure 2. The TA spectra were taken in the indicated solvents at various delay times in the visible (400−800 nm) and NIR (800−1600 nm) spectral ranges.

Laser excitation causes an instantaneous bleaching of the ground state absorption and a build-up of the excited state absorption band (ESA) in the NIR at ∼900 nm. The resulting ESA decays very rapidly to form an intense and narrow ESA peak at 536 nm in *n*-hex (547 nm in THF and ACN). The spectral features on the long wavelength side of that peak are very weak in *n*-hex (Figure 2A) but become more prominent as the polarity of the solvent increases (Figure 2D, G). Simultaneously with the buildup of the ESA, two additional peaks appear in the NIR range: a weak, narrow one at ∼880 nm and a very broad feature peaking at ∼1100 nm and extending beyond 1200 nm. In the nonpolar solvent, *n*-hex (Figure 2A), the short wavelength TA band dominates; however, upon increasing the solvent polarity, the amplitude of this band gradually decreases, and a longer-wavelength, broader feature becomes more prominent (∼620 nm). In the most polar solvent, ACN (Figure 2G), the two TA bands have comparable intensities.

Increasing the solvent polarity also influences the spectral features observed in the NIR range. The small dip at 950 nm, which is barely noticeable in *n*-hex (Figure 2B), becomes much larger in THF (Figure 2E) and dominates in the ESA spectra (after decay of the short-lived TA band at 880 nm) taken in

dx.doi.org/10.1021/jp400038k | J. Phys. Chem. B XXXX, XXX, XXX−XXX

ACN (Figure 2H). A similar band has been observed for a number of ketolated carotenoids and has been assigned to stimulated emission from an ICT state induced by the incident white light from the probe beam.[6−10,13] The TA spectra of C_{39}-peridinin recorded in 2-MTHF at 77 K (Figure 2J, K) are very similar to those obtained in THF at RT (Figure 2D, E). Despite that fact that low temperature leads to narrowing of vibronic bands in the bleaching of the ground state absorption, which is consistent with what is observed in the steady-state absorption spectra (Figure 1), enhancement of vibronic resolution is not observed in the ESA bands in the visible region, which even at 77 K, remain broad. However both the S_1 ($2^1A_g^-$) → S_n and ICT → S_n ESA bands are shifted to longer wavelength by ∼15 nm.

The time-resolved fluorescence 2D contours and DAS profiles obtained from global fitting of the TRF data of C_{39}-peridinin are shown in Figure 2C, F, I, and L. Because in this molecule both S_2 ($1^1B_u^+$) and S_1 ($2^1A_g^-$) excited states are emissive in *n*-hex, the results of global fitting (DAS) can be assumed to correspond to the fluorescence spectra from the individual states. Thus, the short-lived DAS (blue in Figure 2C, F, I, and L) represents the long-wavelength tail of the S_2 ($1^1B_u^+$) → S_0 ($1^1A_g^-$) fluorescence, whereas the long-lived DAS (red in Figure 2C, F, I, and L) corresponds to the S_1 ($2^1A_g^-$) → S_0 ($1^1A_g^-$) fluorescence. Upon solvent polarity increase, the fluorescence spectrum shifts toward longer wavelengths, and substantial loss of vibronic resolution occurs. This is in agreement with previous reports of steady-state fluorescence spectra in various solvents.[14] The fluorescence spectrum (DAS) taken at 77 K (Figure 2L) consists of well-resolved vibronic bands similar to that measured in the nonpolar solvent, *n*-hex (Figure 2C). It is a bit surprising, however, that at 77 K, the ESA spectrum has properties characteristic of the moderately polar solvent (compare Figure 2D and J), but the fluorescence line shape recorded at 77 K is similar to that observed in the nonpolar solvent, *n*-hex (compare Figure 2C and L).

The ESA spectra, time-resolved fluorescence 2D contours, and TRF DAS obtained for peridinin upon excitation into its S_2 ($1^1B_u^+$) state are shown in Supporting Information (SI) Figure S1. This molecule has been extensively studied in the visible range in many solvents; however, investigations of its spectral features in the NIR range have been limited to either very polar (methanol) or nonpolar (*n*-hex) solvents.[11−13] The TA spectra of peridinin reveal features at 650 nm attributable to an ESA from the ICT state, even in the nonpolar solvent *n*-hex.

Also in this solvent, in the NIR range, the spectral profiles barely dip below zero, demonstrating that very little stimulated emission from the ICT state is detectable. In THF, where the TA bands associated with transitions from the S_1 ($2^1A_g^-$) and ICT states at 534 and 640 nm, respectively, have nearly equal amplitudes, broad SE from the ICT state is also clearly seen around ∼910 nm. Transient absorption spectra of peridinin taken at 77 K (SI Figure S1J and K) reveal the typical ICT → S_n spectral line shape with broad band at 670 nm and prominent SE from the ICT state at ∼900 nm; however, the transient signal persists for hundreds picoseconds, which is exceptionally long compared with the data from ACN or even THF. The fluorescence spectrum of peridinin measured in *n*-hex (DAS in SI Figure S1C) does not show as much vibronic resolution as C_{39}-peridinin does (Figure 2C). Upon increasing the solvent polarity, the fluorescence maximum shifts to longer wavelengths from ∼720 nm in *n*-hex to 760 nm in ACN; however, the fluorescence spectrum of peridinin at 77 K (SI Figure S1L) demonstrates well-resolved vibronic features (compare with SI Figure S1C, F, and I).

Even more dramatic than seen for peridinin is the dependence on solvent polarity of the TA spectra of C_{35}-peridinin (SI Figure S2). In *n*-hex (SI Figure S2A), the TA band associated with transition from the S_1 ($2^1A_g^-$) state at 486 nm is already significantly smaller than that observed for peridinin (SI Figure S1A), and in THF (SI Figure S2D), the band is reduced to a small shoulder on a broader feature that appears at ∼580 nm. In THF (SI Figure S2E), a strong emissive band is present at ∼870 nm. The ESA spectra taken in 2-MTHF at 77 K have a very pronounced feature at 640 nm attributable to the ICT state ESA that is red-shifted compared with ACN and THF, but unlike in these two solvents, it persists for a few nanoseconds. The influence of the ICT state is also apparent in the fluorescence spectrum of C_{35}-peridinin taken in *n*-hex, in which the vibronic structure is barely noticeable (DAS in SI Figure S2C). In THF and ACN (SI Figure S2F and I), the fluorescence spectra are essentially featureless. In addition, only a small enhancement in the vibronic resolution is observed as the temperature is lowered to 77 K (SI Figure S2L).

The shortest analogue, C_{33}-peridinin, demonstrates the most striking polarity dependence of the spectral properties of all the molecules (SI Figure S3). In *n*-hex, only one wide-ranging TA band with maximum at 610 nm is evident in the visible region (SI Figure S3A), and it has a characteristic ICT state appearance. However, SE in the NIR is not present in this solvent, or it is hidden underneath coinciding ESA bands. The SE appears prominently at ∼800 nm in THF (SI Figure S3E), but it is distorted by overlapping with a sharp TA band at 800 nm. Stimulated emission is also clearly noticeable as a negative band in the TA spectrum in the visible spectral region (SI Figure S3D) down to ∼600 nm. In ACN, SE dominates in both spectral ranges (SI Figure S3H, G) and exhibits broad and featureless lineshapes typical of an ESA transition from the ICT state.

The 77 K TA spectra of C_{33}-peridinin (SI Figure S3J) have characteristics similar to those recorded for C_{35}-peridinin (SI Figure S2J). The spectral bands persist for a few nanoseconds, and furthermore, show the presence of a strong stimulated emission in the NIR with its most pronounced feature at ∼820 nm. However, a precise determination of the SE position is precluded because of overlapping of the SE band with the TA bands also present in this range.

The fluorescence spectra of C_{33}-peridinin shown in SI Figure S3C, F, I, and L are devoid of vibronic resolution in all solvents, even at 77 K. The major difference between the 77 K and RT fluorescence spectra is the position of the band maximum, which appears ∼40 nm to shorter wavelength at the low temperature (600 nm in ACN vs 560 nm in 2-MTHF at 77 K).

"Forbidden" S_0 ($1^1A_g^-$) → S_1 ($2^1A_g^-$) Absorption. A closer look at the steady-state absorption spectra from Figure 1 reveals additional small absorption bands present on the long-wavelength side of the S_0 ($1^1A_g^-$) → S_2 ($1^1B_u^+$) transition.

A detailed analysis of steady-state absorption spectra of series of peridinin analogues taken in 2-MTHF at 77 K is shown in Figure 3.

It is generally assumed that the vibronic structure of the S_0 ($1^1A_g^-$) → S_2 ($1^1B_u^+$) electronic transition of polyenes and carotenoids can be modeled as combinations of progressions of two vibrational modes with frequencies of ∼1200 cm^{-1} (totally symmetric C−C stretching vibrations) and ∼1600 cm^{-1} (totally symmetric C═C stretching vibrations); however, recent

dx.doi.org/10.1021/jp400038k | J. Phys. Chem. B XXXX, XXX, XXX−XXX

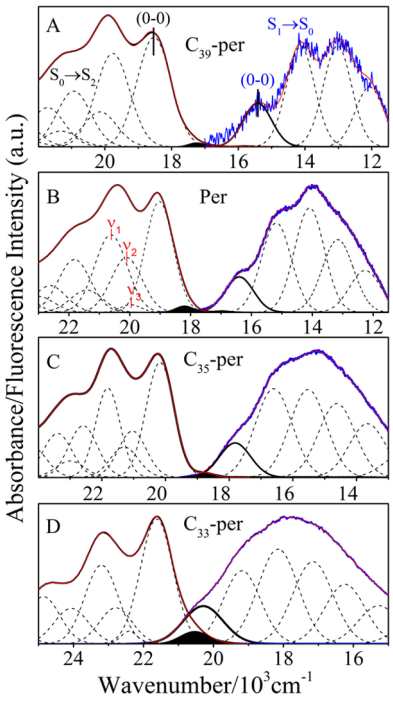

Figure 3. The steady-state S_0 ($1^1A_g^-$) → S_2 ($1^1B_u^+$) absorption spectra overlaid with TRF profiles representing S_1 ($2^1A_g^-$) → S_0 ($1^1A_g^-$) fluorescence emission spectra of the peridinin analogues recorded in 2-MTHF at 77 K and showing reconstructed vibronic structure. The vibronic bands were generated by Gaussian functions. The position of the (0−0) vibronic band in both absorption and emission spectra is indicated. The ν_1, ν_2, and ν_3 labels denote the principal vibronic modes contributing to the vibronic progression of the S_0 ($1^1A_g^-$) → S_2 ($1^1B_u^+$) absorption band. See the main text and Table 1 for more detailed information about the fitting procedure and results.

Raman spectroscopic studies of peridinin dissolved in various solvents and crystallized into the solid state as well as theoretical computations[26,27] argued that the Raman spectrum is dominated by three modes: C═C symmetric stretching (∼1520 cm^{-1}) (ν_1), C−H deformation methine bridges (∼1130−1190 cm^{-1}) (ν_2), and C−O stretching (∼940 cm^{-1}) (ν_3), in which two first appeared to be the most pronounced. Thus, the ground state absorption spectrum may be successfully reconstructed on the basis of a progression of these modes, at least in the case of peridinin. We have not applied a strict Franck−Condon analysis for spectral reconstruction, but we have performed a simple sum of Gaussian functions mimicking the progression of the vibronic modes. The results of reconstructing the absorption spectra are shown in Figure 3. The parameters pertaining to the individual components of the spectra and their assignments are given in Table 1.

The widths of the Gaussian profiles associated with either ν_1, ν_2, or their linear combinations were kept similar to the width of the (0−0) vibronic band. One exception was for the Gaussian associated with the ν_3 band, which was taken to be narrower. This is based on the assumption that the number of possible ν_1 or ν_2 nearly degenerate modes associated with different parts of the carbon skeleton collectively form broader vibronic motions, much larger than those for ν_3, whose number of nearly degenerate vibrations is limited. In general, reconstructions obtained for the absorption spectra were very precise. For C_{39}-peridinin and peridinin, the ν_1 and ν_2 modes obtained from the fitting very closely match those from the resonance Raman experiments. In the case of C_{39}-peridinin, the ν_3 mode was not needed to obtain a satisfactory reconstruction. For C_{35}- and C_{33}-peridinin, ν_2 differs from that obtained for the longer analogues but still falls within the expected range of a

Table 1. Parameters for the Reconstruction of the Absorptive and Emission Spectra of Peridinin and Analogues in 2-MTHF at 77 K

state parameters			carotenoid			
state	vibronic band	mode assignment	C_{39}-per	peridinin	C_{35}-per	C_{33}-per
			Fluorescence			
S_1 ($2^1A_g^-$)	(0−0) (fwhm)	n.a	15 420 (1000)	16 400 (1100)	17 820 (1150)	20 290 (1330)
			Absorption			
S_2 ($1^1B_u^+$)	(0−0)	n.a.	18 520	19 060	20 170	21 620
	(0−1)	(0−0) + ν_3	ne	19 980	21 040	22 410
		(0−0) + ν_2	19 760	20 210	21 300	22 790
		(0−0) + ν_1	20 110	20 550	21 810	23 200
	(0−2)	(0−0) + 2ν_2	20 890	21 390	22 590	24 060
		(0−0) + ν_1 + ν_2	21 230	21 730	22 990	ne[a]
		(0−0) + 2ν_1	21 570	22 070	23 390	24 870
	(0−3)	(0−0) + 3ν_2	22 090	22 620	ne[a]	ne[a]
		(0−0) + 2ν_2 + ν_1	22 750	22 950	24 190	25 860
		(0−0) + 3ν_1	23 090	23 620	24 990	26 610
⟨fwhm⟩[b]			1 190	1 180	1 040	1 110
			⟨ν_1⟩ = 1 540	⟨ν_1⟩ = 1 510	⟨ν_1⟩ = 1 620	⟨ν_1⟩ = 1 620
			⟨ν_2⟩ = 1 195	⟨ν_2⟩ = 1 170	⟨ν_2⟩ = 1 170	⟨ν_2⟩ = 1 190
				ν_3 = 920	ν_3 = 870	ν_3 = 790
⟨ν_i⟩[c]				(800)	(800)	(800)
			Additional Peaks in Absorption Spectra			
peak position (fwhm)			17 240 (580)	17 020 (700)	18 720 (620)	20 540 (970)
				18 190 (700)		

[a]ne, not evident. [b]fwhm = full width at half-maximum. [c]Average values.

dx.doi.org/10.1021/jp400038k | J. Phys. Chem. B XXXX, XXX, XXX−XXX

C═C symmetric stretch. As the π-chain length shortens, the ν_3 mode shifts considerably to lower frequency by ~200 cm^{-1}.

In addition, the Gaussian fits of the absorption spectra revealed weak bands on the long wavelength side of the S_0 $(1^1A_g^-) \rightarrow S_2$ $(1^1B_u^+)$ absorption spectra (Figure 3) that do not match the vibronic progression of this transition. If the energy of these weak bands is plotted along with the spectral origin (0−0 band) of the S_0 $(1^1A_g^-) \rightarrow S_2$ $(1^1B_u^+)$ transition, it is clearly evident that the resulting straight lines do not have the same slope. This strongly suggests that these weakly allowed bands are not associated with the same electronic transition as the main peaks. The intensity distribution is reminiscent of the well-studied case of nonadiabatic coupling between the S_1 $(2^1A_g^-)$ and S_2 $(1^1B_u^+)$ states in diphenyloctatetraene.[28,29] Furthermore, Wang et al[30] reported steady-state absorption spectra of a series of highly concentrated (OD ~ 15−20 in a 1 cm path cuvette at the maximum of the S_0 $(1^1A_g^-) \rightarrow S_2$ $(1^1B_u^+)$ band) open-chain carotenoids from purple bacteria having N values from 8 to 13, and argued on the basis of a Gaussian reconstruction of the spectral profiles, that a very weak S_0 $(1^1A_g^-) \rightarrow S_1$ $(2^1A_g^-)$ transition is present in the long wavelength tail of the (0−0) vibronic band of the strongly allowed S_0 $(1^1A_g^-) \rightarrow S_2$ $(1^1B_u^+)$ spectrum. The S_1 $(2^1A_g^-)$ energy values obtained in that analysis were very reasonable, but at such high concentrations, one has to be wary of the potential of carotenoids to form aggregates.

In the present experiments, the samples were used directly after purification by HPLC and had an OD (in a 1 cm path at the λ_{max}) between 0.3 and 0.8 and very good solubility in 2-MTHF-minimizing aggregate formation. In addition, the amplitudes of the weak absorption bands seen here for the peridinin analogues are higher by a few orders of magnitude compared with the signals observed by Wang et al.[30] The presence of low energy bands in the absorption and relatively strong fluorescence from the S_1 $(2^1A_g^-)$ (see Figure 3) state suggest that the constraints imposed by the symmetry selection rules for the electronic transition between the S_0 $(1^1A_g^-)$ and S_1 $(2^1A_g^-)$ states are less severe for peridinin and the analogues than for open-chain carotenoids. This is undoubtedly related to the lack of molecular symmetry in the peridinin molecules.

If the positions of these new bands are plotted simultaneously with positions of the S_1 $(2^1A_g^-) \rightarrow S_0$ $(1^1A_g^-)$ fluorescence spectra recorded at 77 K (Figure 4), it is clear that the best fit lines representing the positions of the weak absorptive bands and those representing fluorescence (0−0) vibronic bands are almost collinear.

At first glance, such collinearity strongly suggests that both sets of bands are associated with the same excited state. Because the fluorescence occurs from the one photon-forbidden S_1 $(2^1A_g^-)$ state, the weak absorption bands must then be associated with the S_0 $(1^1A_g^-) \rightarrow S_1$ $(2^1A_g^-)$ transition, and the energy difference of 300−600 cm^{-1} between the (0−0) vibronic bands of the hypothetical S_0 $(1^1A_g^-) \rightarrow S_1$ $(2^1A_g^-)$ absorption and fluorescence can be accounted for a typical Stokes shift observed for carotenoids.[30,31] Because the energy gap between the S_1 $(2^1A_g^-)$ and the S_2 $(1^1B_u^+)$ states is greatly reduced due to downshift of S_0 $(1^1A_g^-) \rightarrow S_2$ $(1^1B_u^+)$ transition, the forbidden S_0 $(1^1A_g^-) \rightarrow S_1$ $(2^1A_g^-)$ absorption becomes more allowed due to electronic mixing of the S_1 $(2^1A_g^-)$ and S_2 $(1^1B_u^+)$ excited states. This is modeled by first-order perturbation theory and the assumption that the energies of the vibronic levels of the S_1 $(2^1A_g^-)$ state are all lower than the energy of the first vibronic level of the S_2 $(1^1B_u^+)$ state. A

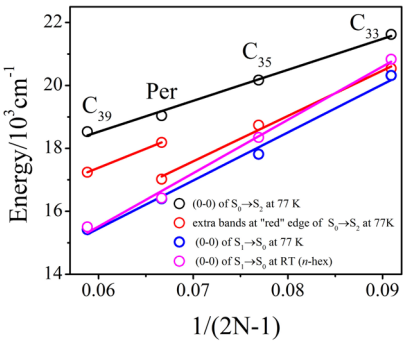

Figure 4. Electronic state energy diagram based on the spectral reconstruction shown in Figure 3. The higher energy vibronic bands of the S_0 $(1^1A_g^-) \rightarrow S_2$ $(1^1B_u^+)$ transition were omitted for clarity. The diagram shows points taken in 2-MTHF at 77 K. Data also provided in *n*-hex at room temperature.

nonzero transition dipole moment of each vibronic band, ν, of the S_0 $(1^1A_g^-) \rightarrow S_1$ $(2^1A_g^-)$ absorption can be computed from the expression:[30]

$$\mu_{S_1(\nu=0,..,n)} \approx \mu^{(0)}_{S_1(\nu=0)} + \mu^{(0)}_{S_2(\nu=0)} \frac{\left\langle \Psi^{(0)}_{S_2(0)} | V | \Psi^{(0)}_{S_1(0)} \right\rangle}{E_{S_1(\nu=0,..,n)} - E_{S_2(0)}} \times \frac{1}{\left\langle \chi_{S_2(0)} | \chi_{S_1(0)} \right\rangle} \quad (1)$$

where $\mu^{(0)}_{S_1(\nu=0)}$ is the transition dipole moment for the unperturbed S_1 $(2^1A_g^-)$ state, $\mu^{(0)}_{S_2(\nu=0)}$ is the transition dipole moment for the (0−0) vibronic level of an unperturbed S_2 $(1^1B_u^+)$ state, and V is perturbation that mixes the S_1 $(2^1A_g^-)$ and the S_2 $(1^1B_u^+)$ states. $\Psi^{(0)}_{S_2(0)}$ and $\Psi^{(0)}_{S_1(0)}$ are electronic wave functions, and $\chi_{S_2(0)}$ and $\chi_{1(0)}$ are vibronic wave functions of the zero-order, unperturbed S_2 $(1^1B_u^+)$, and S_1 $(2^1A_g^-)$ states, respectively. The model assumes that the perturbation is induced by the first vibronic level of the S_2 $(1^1B_u^+)$ state. The influence of all higher vibronic levels is neglected. Because $\mu^{(0)}_{S_1(\nu=0)} = 0$, an induced transition dipole moment and, correspondingly, the oscillator strength of the transition will be dependent on the energy gap between the *n*th vibronic band of the S_0 $(1^1A_g^-) \rightarrow S_1$ $(2^1A_g^-)$ transition and the (0−0) vibronic band of the S_0 $(1^1A_g^-) \rightarrow S_2$ $(1^1B_u^+)$ transition. The smaller the energy difference between these two vibronic bands, the larger will be their amplitudes. Thus, the effect should be clearly evident in the low-temperature absorption spectra. The spectral shift caused by low temperature narrows the S_2 $(1^1B_u^+) - S_1$ $(2^1A_g^-)$ energy gap by ~1000 cm^{-1}, and this increases the value of the transition dipole moment for the S_0 $(1^1A_g^-) \rightarrow S_1$ $(2^1A_g^-)$ transition by more than a factor of 2, assuming all other factors remain constant.

The S_2 $(1^1B_u^+)/S_1$ $(2^1A_g^-)$ state mixing should be resolved in Stark spectra for these molecules. Coupling of higher-lying B_u states absorbing at ~270 nm with another electronic state, purportedly the $2^1A_g^-$ state, was recently suggested for a few carotenoids on the basis of steady-state and Stark absorption measurements.[32] However, the coupling of the S_2 $(1^1B_u^+)$ state with the S_1 $(2^1A_g^-)$ state in peridinin has not yet been demonstrated by Stark spectroscopy,[33] and Stark spectroscopy results of peridinin analogues have not been published in detail.[21] This subject still remains open.

dx.doi.org/10.1021/jp400038k | J. Phys. Chem. B XXXX, XXX, XXX−XXX

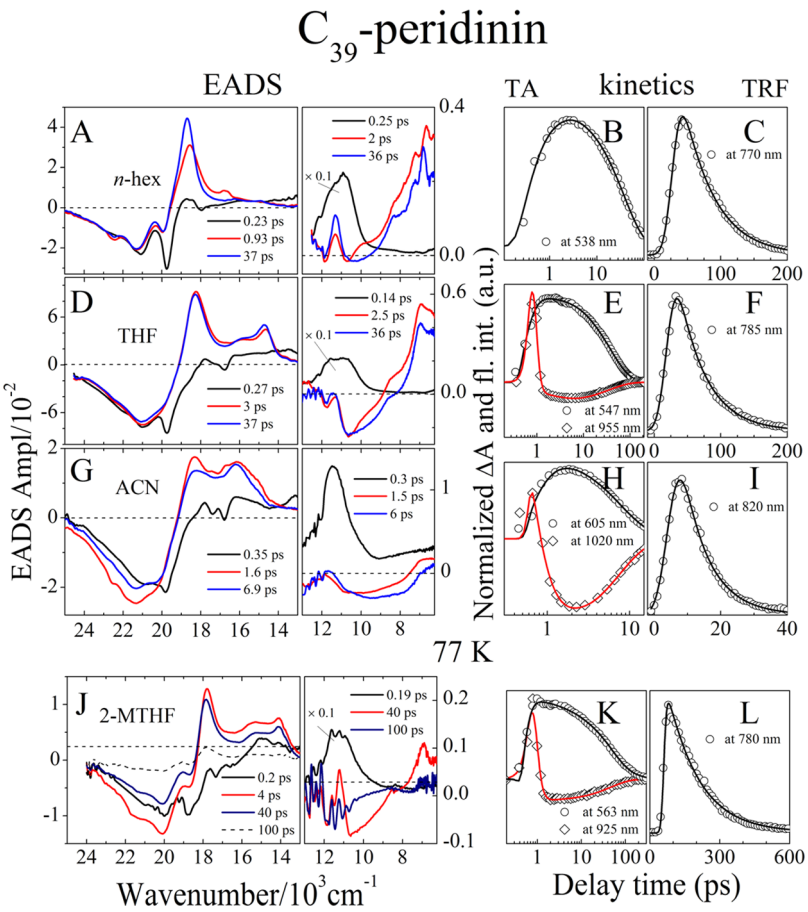

Figure 5. Global fitting results of the TA data sets, the representative kinetic traces extracted from the TA with the accompanying fits, and the fluorescence decay kinetics extracted from the fluorescence time-resolved profiles of C_{39}-peridinin.

It is generally assumed that temperature does not influence energy of the S_1 ($2^1A_g^-$) state of carotenoids. However, this is not the case for the carotenoids studied here. Figure 4 shows the energy of the S_1 ($2^1A_g^-$) state of the peridinin analogues obtained from fluorescence measurements in *n*-hex at RT (magenta).[14] For the longest analogue (C_{39}-per), the S_1 ($2^1A_g^-$) state energy essentially does not change with lowering the temperature. However, for the shortest analogue (C_{33}-per), lowering the temperature shifts the energy of the S_1 ($2^1A_g^-$) state to lower energy by ~600 cm^{-1}. It can be explained by assuming that the S_1 ($2^1A_g^-$) state is more perturbed by the S_2 ($1^1B_u^+$) for shorter analogues because of a smaller energy gap between both states at RT. It will result in a larger value of μ_{S_1} and, ultimately, greater sensitivity of the S_1 ($2^1A_g^-$) state for changes of the molecule environment, in this case, change of solvent polarizability if the temperature is lowered to 77 K. Under conditions that the S_2 ($1^1B_u^+$) state of all of the analogues shifts to lower energy by ~1000 cm^{-1}, the S_2 ($1^1B_u^+$) − S_1 ($2^1A_g^-$) energy gap narrowing that occurs upon lowering the temperature will be less for the shortest analogue, C_{33}-peridinin (~400 cm^{-1}), than for peridinin and C_{39}-peridinin (~1000 cm^{-1}). Therefore, enhancement of the hypothetical S_0 ($1^1A_g^-$) → S_1 ($2^1A_g^-$) absorption band may be different for each analogue in the series and may not demonstrate any specific trend.

The Stokes shift (in cm^{-1}) observed between the purported S_0 ($1^1A_g^-$) → S_1 ($2^1A_g^-$) absorption and the S_1 ($2^1A_g^-$) → S_0 ($1^1A_g^-$) fluorescence should at least to a first approximation follow the Lippert−Mataga equation,[34] which is given by

$$\Delta\bar{\nu} = C_1\left(\frac{\varepsilon - 1}{2\varepsilon + 1} - \frac{n^2 - 1}{2n^2 + 1}\right)\frac{\Delta\mu}{a^3} \quad (2)$$

where C_1 is a constant, ($[(\varepsilon - 1)/(2\varepsilon + 1)] - [(n^2 - 1)/(2n^2 - 1)]$) is the orientation polarizability; n and ε are the refractive index and dielectric constant of the solvent, respectively; $\Delta\mu$ is the change in dipole moment between the S_1 ($2^1A_g^-$) and S_0 ($1^1A_g^-$) states; and a is a radius of the fluorescing molecule (approximated by a sphere). According to this equation, for 2-MTHF, which has the substantial orientation polarizability at 77 K of ~0.16 (n = 1.8 and ε = 19), the Stokes shift should be different for each molecule in the series. Presumably, it would be smallest for C_{39}-peridinin (small $\Delta\mu$ due to weak state mixing and the largest molecule volume) and the largest for C_{33}-peridinin (larger $\Delta\mu$ due to stronger state mixing and the smallest molecule volume). However, the observed shift between the presumed S_0 ($1^1A_g^-$) → S_1 ($2^1A_g^-$) absorption and the S_1 ($2^1A_g^-$) →S_0 ($1^1A_g^-$) fluorescence shows the opposite trend (see Figure 4): ~250 cm^{-1} for C_{33}-peridinin and 580 cm^{-1} for peridinin. This suggests that the assignment of the weak bands may not be to the forbidden S_0 ($1^1A_g^-$) → S_1 ($2^1A_g^-$) transition; however, the predicted trend may be simply over idealized. As was pointed out earlier in the text, it is unclear that $\Delta\mu$ has a clear trend at 77 K (e.g., larger for shorter molecule).

dx.doi.org/10.1021/jp400038k | J. Phys. Chem. B XXXX, XXX, XXX−XXX

Table 2. Dynamics of the Excited States of C_{39}-Peridinin, Peridinin, C_{35}-Peridinin and C_{33}-Peridinin Determined by Global Fitting of the Transient Absorption Data Sets and Fitting of the Single Wavelength Kinetics for the Time-Resolved Fluorescence Experiments[a]

		transient absorption range										
		visible				NIR				TRF		
molecule	solvent	τ_1(ps)	τ_2(ps)	τ_3(ps)	τ_4(ps)	τ_1(ps)	τ_2(ps)	τ_3(ps)	τ_4(ps)	τ_{F1}(ps)	τ_{F2}(ps)	ref
C_{39}-per	*n*-hex	0.23	0.93	37		0.25	2.0	36		<IRF	46	this work
		0.20	1.7	41.2								14
	THF	0.27	3.0	37		0.40	2.5	36		41		this work
	ACN	0.35	1.6	6.9		0.30	1.5	6.0		8.3		this work
	2-MTHF	0.20	4.0	40	100	0.19	n.e.[c]	40	100	<IRF	130	this work
peridinin	*n*-hex	0.44	4.5	155	inf[b]	0.35	6.0	168		200		this work
				160								13
				160								11
				161						156		12
				161								4
		<0.17	1.4	186								14
	THF	0.23	0.80	80		0.40	2.2	77		94		this work
	ACN	0.20	0.90	5.0	8.5	0.11	0.67	8.3		10		this work
					8.5							11
					7.9–8.3							13
					9							4
	2-MTHF	0.53	13	180		0.28	15	168		240		this work
C_{35}-per	*n*-hex	0.35	95	890	inf	0.30	7.0	200	970	960		this work
		0.21	70	1000								14
	THF	0.28	2.1	38	105	0.50	2.4	32	95	30	110	this work
	ACN	0.25	2.1	11		0.33	5.8			12.5		this work
	2-MTHF	0.17	1.0	448		ne	ne	450		860		this work
C_{33}-per	*n*-hex	0.16	140	3700	inf	0.25	320	3100		830	3900	this work
		0.22	130	4200								14
	THF	0.30	2.4	5.8	32	0.25	1.4	6.9	34	<IRF	46	this work
	ACN	0.36	2.9	9.8		0.21	2.6	11.5		6.5		this work
	2-MTHF	0.58	390	1720		0.21	230	1800		1800		this work

[a]The uncertainties do not exceed 10% of the fitted values. [b]inf, infinity. [c]ne, not evident; THF, tetrahydrofuran; ACN, acetonitrile; 2-MTHF, 2-methyltetrahydrofuran (77 K); IRF, instrument response function.

Excited States Dynamics. The results of global fitting of the TA data sets and representative kinetics traces of TA and TRF of C_{39}-peridinin are shown in Figure 5.

The TA data recorded in the visible and NIR ranges were converted to wavenumber units and fit separately. The goodness of fit of the TA data is demonstrated in Figure 5B, E, H, and K, in which the representative single wavelength kinetics are overlaid with corresponding fits obtained from global fitting. The time delay axis is shown on a logarithmic scale to enhance clarity over the long time span. Independent fitting procedures in the NIR and visible spectral ranges led to very similar lifetimes of the kinetic components, suggesting that the same spectral species are observed in both ranges. The EADS components can be explained on the basis of the temporal and spectral properties as follows: The shortest EADS with the lifetime between 0.14 and 0.35 ps is associated with the decay of the S_2 ($1^1B_u^+$) state. This is consistent with the instantaneous (within the time resolution of the TA spectrometer) appearance of ground state bleaching in the visible region between 19 000 and 24 000 cm^{-1} and the simultaneous rise of the TA band in the NIR at ~11 000 cm^{-1} that is known to be associated with the S_2 ($1^1B_u^+$) → S_n transition reported previously for a number of carotenoids.[35−37] This spectral species decays to form another component having a lifetime from 0.93 ps in *n*-hex to 4 ps in 2-MTHF (77 K). The shape of this EADS, especially in *n*-hex, suggests that it is associated with a nonequilibrated, vibronically hot S_1 ($2^1A_g^-$) state.[36−40]

The scheme is more complicated in polar solvents in which the S_1 ($2^1A_g^-$) and ICT states coexist. In this case, it is possible that the observed lineshapes belong to a mixture of non-equilibrated S_1 ($2^1A_g^-$) and ICT states. The second EADS evolves to form a third kinetic component that is most sensitive to solvent polarity. In the nonpolar solvent, *n*-hexane, and the moderately polar solvent, THF, this component has the same 37 ps lifetime. However, in the polar solvent, ACN, this value decreases to ~6.4 ps, the average of fitting results from data taken in the visible and NIR ranges. The fitting results for C_{39}-peridinin in 2-MTHF taken at 77 K are very similar to those obtained for *n*-hex and THF except that another kinetic component is necessary to obtain a satisfactory fit. The lifetime of this final component is 100 ps, and its spectral shape is very similar to that of the third component. Because the S_1 ($2^1A_g^-$) state lifetime is 37 ps and unaffected by solvent polarity, this long-lived EADS component may be due to an alternative conformation of the molecule that is frozen in at cryogenic temperatures and which has a longer S_1 ($2^1A_g^-$) state lifetime compared with that at RT. Similar observations have been reported for xanthophylls and open-chain carotenoids.[38,40]

The kinetic traces together with fits obtained from global fitting of the fluorescence decay profiles of C_{39}-peridinin in the different solvents (Figure 2C, F, I, L) are shown in Figure 5C,

dx.doi.org/10.1021/jp400038k | J. Phys. Chem. B XXXX, XXX, XXX−XXX

F, I, L. The lifetimes are in reasonable agreement with the time constants of the longest EADS components obtained from the TA data sets (Figure 5A, D, G, F). All of the results obtained from fitting the decay dynamics of C_{39}-peridinin are summarized in Table 2.

The results of global fitting the TA data sets recorded from peridinin in the various solvents are shown in SI Figure S4. The kinetic components follow trends similar to those for C_{39}-peridinin with a few notable exceptions: Fitting the peridinin TA data recorded in *n*-hex in the visible range revealed a very weak EADS component having a very long lifetime (green trace in SI Figure S4A).

The spectral shape and "infinite" lifetime are suggestive of its being associated with the formation of an excited triplet state.[41,42] In addition, the EADS traces for peridinin in 2-MTHF at 77 K are very different from those seen for C_{39}-peridinin. Most noticeable in SI Figure S4J is that the TA bands have broad, ICT-like spectral characteristics. On this basis, it may be expected that the final EADS component associated with the ICT state may have a short lifetime. However, this is not the case. The obtained value of 180 ps is longer than the lifetime of the S_1 ($2^1A_g^-$) state measured in *n*-hex. Moreover, the stimulated emission band seen in the NIR range decays in 168 ps, which is similar to the 180 ps value obtained from the TA experiment in the visible range.

The global fitting results of the TA spectra of C_{35}-peridinin are shown in SI Figure S5. In *n*-hex, the lifetime of the equilibrated S_1 ($2^1A_g^-$) state of 890 ps obtained from TA or 970 ps from TRF is in good agreement with the value of 1 ns obtained previously using time-correlated single-photon counting (TCSPC) methods.[14]

As was observed for peridinin, global fitting of the TA data sets revealed the presence of a nondecaying component (green trace in SI Figure S5A). Again, the spectral shape of this EADS resembles the transient spectrum of the excited triplet state that can be generated in *n*-hex using triplet photosensitizers.[41] The kinetic components of C_{35}-peridinin are strongly dependent on solvent polarity. The TA data recorded in THF (SI Figure S5E) reveals two EADS with similar spectral characteristics but different amplitudes and different lifetimes of 38 and 105 ps. In ACN (SI Figure S5G), the longest-lived component is associated with the ICT state lifetime that has an average value from the VIS and NIR data of 8.4 ps. The global fitting results for C_{35}-peridinin recorded in 2-MTHF at 77 K in the visible range revealed three kinetic components with lifetimes of 170 fs and 1 and 448 ps. The last two EADS have essentially the same spectral shapes (SI Figure S5J). In the NIR range, global fitting revealed only one kinetic component with a lifetime matching the longest EADS obtained in the visible region.

Global fitting of the TA results from C_{33}-peridinin are shown in SI Figure S6. A good fit of the data set recorded in *n*-hex in the visible range required four kinetic components with lifetimes of 0.16 ps, 140 ps, 3.7 ns and infinity.

The lifetime of the equilibrated S_1 ($2^1A_g^-$) state is in reasonable agreement with the value of 4.2 ns obtained previously from measurements using TCSPC.[14] As was observed for peridinin and C_{35}-peridinin, global fitting of the TA data sets revealed the presence of a nondecaying component (green trace in SI Figure S6A) with a spectral shape resembling the transient spectrum of the excited triplet state that can be generated in *n*-hex using triplet photosensitizers.[41] It is also apparent that the amplitude of the excited triplet state ESA increases while the lifetime of the S_1 ($2^1A_g^-$) gets longer. The lifetime of the ICT state in ACN is 9.8 ps, based on the kinetics of the ESA in the visible region.

An interesting result from the global fitting of the TA data sets is the fact that these carotenoids (excluding C_{39}-peridinin) exhibit transient spectra associated with photoinduced triplet states even in the absence of a triplet sensitizer. Typically, the yield of triplet states for a carotenoid in solution is very small because of strong competition from internal conversion of the S_1 ($2^1A_g^-$) state to the ground state. Typical quantum yields of triplet state formation, Φ_T, are less than 10^{-3}.[43] For the molecules studied here, the quantum yields can be obtained by taking a ratio of the amplitudes of bleaching of the ground state absorption at time zero compared with a time when only the contribution from the triplet state is observed in the ESA. This results in $\Phi_T = 2 \times 10^{-3}$ for peridinin. However, for C_{35}-peridinin and C_{33}-peridinin, the values are higher at 7×10^{-3} and 4.6×10^{-2}, respectively. A mathematical analysis demonstrates that Φ_T depends exponentially on the reciprocal of the number of conjugated carbon−carbon double bonds in the carotenoid π-electron chain; that is, by the equation $\ln(\Phi_T) = A + B/(2N + 1)$, where A and B are constants and N is the number of conjugated C=C bonds (Figure 6).

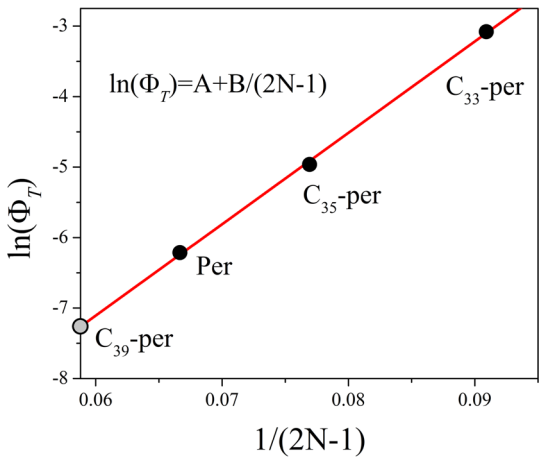

Figure 6. Quantum yields of triplet state formation, Φ_T expressed as a function of the π-electron conjugation (N) of the peridinin analogues, $\ln(\Phi_T) = A + B/(2N - 1)$ where $A = -14.9 \pm 0.3$ and $B = 130 \pm 3$. The yield of the triplet formation for C_{39}-peridinin was predicted by extrapolation of the linear fit to $1/(2N - 1) = 0.059$ ($N = 9$ for C_{39}-peridinin) and is 0.7×10^{-3} ($\ln 0.0007 = -7.26$).

DISCUSSION

Nature of the ICT State. Various models have been advanced to explain the kinetic and spectral behavior of the ICT state in peridinin and other carbonyl-containing carotenoids. One model assumes that the ICT is a separate electronic state that operates independently from S_1 ($2^1A_g^-$).[5,14] The energy of the ICT state is strongly dependent on solvent polarity; that is, the state is stabilized if the solvent polarity increases. In this model, for carbonyl-containing carotenoid in nonpolar solvents, the ICT state energy level is thought to lie above the S_1 ($2^1A_g^-$) state and, therefore, does not significantly affect the TA spectra and excited state dynamics. However, increasing the solvent polarity stabilizes the ICT state such that it crosses the S_1 ($2^1A_g^-$) state and takes on the ability to accept population from it. Thus, the S_1 ($2^1A_g^-$)

dx.doi.org/10.1021/jp400038k | J. Phys. Chem. B XXXX, XXX, XXX−XXX

lifetime is shortened until it reaches a minimum of ~10 ps. Another model assumes that the ICT state is strongly coupled to the S_1 ($2^1A_g^-$) state and exists as a local minimum on its potential energy surface. In this model, the ICT state is a manifestation of the effect of solvent polarity on the S_1 ($2^1A_g^-$) state. The local minimum becomes deeper in energy as the solvent polarity increases, and at very high solvent polarity, it becomes the global minimum. The difficulty in distinguishing these two models is that both cases will lead to the same spectral observations. In addition, on the basis of the similarity of the ICT state lifetimes for different molecules in the polar solvent methanol, it has been suggested that the ICT state does not depend on the extent of π-electron conjugation of a carotenoid;[14] however, this finding was never tested by direct measurements of the SE from the ICT state.

The visible-NIR TA spectra of the four molecules studied here, taken in ACN at 5 ps after excitation, are shown in Figure 7. All spectral profiles show a pronounced negative feature that is associated with SE from the ICT state.

The data indicate that the position of the SE spectrum shifts to higher energy when the π-electron conjugation is shortened (see the values noted in Figure 7). For a better visualization of trend of shift, the spectral line was fitted to a Gaussian profile. The complete visible-NIR TA spectra are also shown in the insets of Figure 7. Plotting the positions of the SE spectra along with other transitions as a function of π-electron conjugation expressed as $1/(2N-1)$ (Figure 8A) demonstrates that

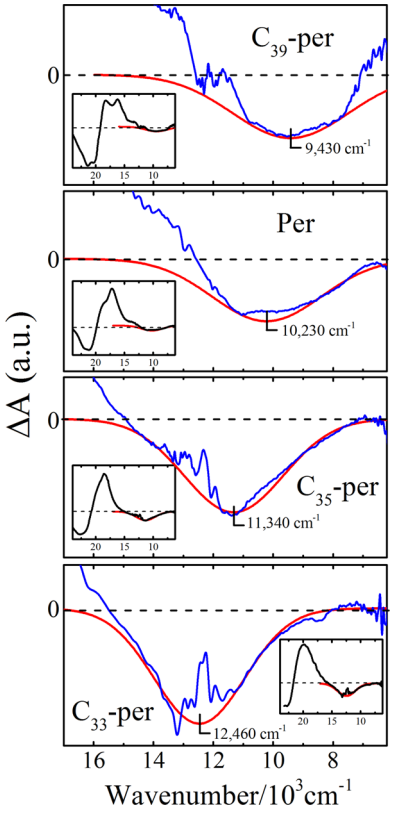

Figure 7. Portions of the TA spectrum of four studied analogues enhancing the SE band from the ICT state. The spectral profiles were extracted from the TA spectra taken in ACN and recorded 5 ps after excitation and are presented on the same scale in a wavenumber notation. Each stimulated emission band was mimicked by the Gaussian profile. The positions of the Gaussians are indicated. In addition, the complete TA spectra (450–1600 nm) (in wavenumber notation) are highlighted in the inserts. Shift of position of the SE band to the higher energies while π-electron conjugation shortens is clearly noticeable.

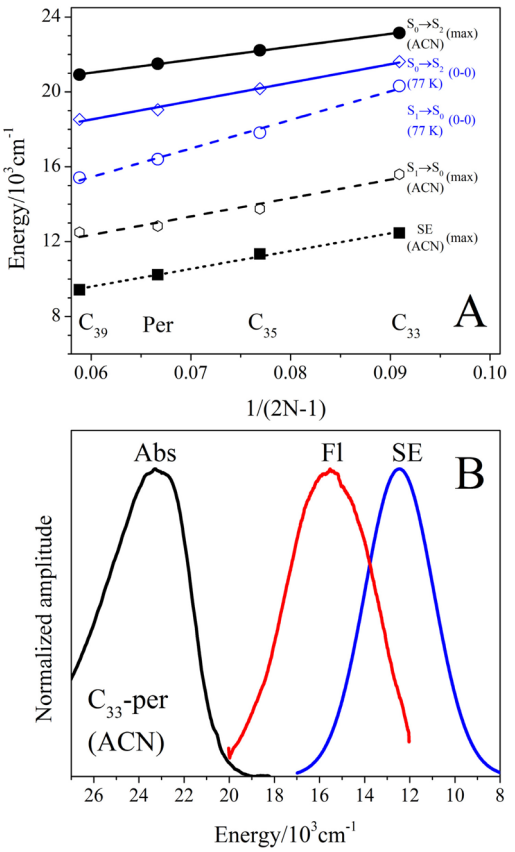

Figure 8. (A) Energy state diagram of positions of the (0–0) vibronic band of the S_0 ($1^1A_g^-$) → S_2 ($1^1B_u^+$) in 2-MTHF (77 K) (with corresponding linear fits) (solid blue), the S_0 ($1^1A_g^-$) → S_2 ($1^1B_u^+$) band maximum in ACN (black), the (0–0) vibronic band of the S_1 ($2^1A_g^-$) → S_o ($1^1A_g^-$) in 2-MTHF (77 K) (dashed blue), the S_1 ($2^1A_g^-$) → S_o ($1^1A_g^-$) fluorescence maximum in ACN and positions of the ICT SE in ACN plotted as a function of conjugated double bonds (N) for studied peridinin analogues. (B) Absorption, fluorescence, and stimulated emission (Gaussian from Figure 7) of C_{33}-peridinin in ACN. The spectral profiles were normalized to identical amplitude and plotted in wavenumber scale for clarity of comparison.

(i) the positions of center of the SE spectra can be very precisely fitted with a linear function, and

(ii) the slopes of the linear fits of the positions of center of the SE spectra and the energies of maximum of the band for the S_1 ($2^1A_g^-$) → S_0 ($1^1A_g^-$) transition measured in ACN are practically identical (95 000 vs 98 000) but very different from the slope of the fit of the energies of the (0–0) vibronic band of the S_1 ($2^1A_g^-$) → S_0 ($1^1A_g^-$) transition at 77 K (153 000) and different from the slope of the linear fit of the positions of maximum of the S_0 ($1^1A_g^-$) → S_2 ($1^1B_u^+$) transition in ACN (69 000).

It was recently suggested that the energy of the ICT state should lie in the vicinity of the S_1 ($2^1A_g^-$) and S_2 ($1^1B_u^+$) states.[44] The studies were performed on the polyeneal 8,8′-diapocarotene-8′-ol-8-al, having seven conjugated carbon–carbon double bonds substituted with carbonyl and hydroxyl groups at the terminal carbons.[44] The data obtained from

dx.doi.org/10.1021/jp400038k | J. Phys. Chem. B XXXX, XXX, XXX–XXX

steady-state absorption, fluorescence, and time-resolved absorption spectroscopy supported by molecular orbital theory and molecular dynamics calculations demonstrate that the ICT state evolves in the polar solvent via mixing of the low-lying S_1 (2^1A_g-like) and S_2 (1^1B_u-like) excited singlet states, with its energy being in the vicinity of the S_1 ($2^1A_g^-$) and S_2 ($1^1B_u^+$) states. The authors proposed that this mechanism of ICT state formation applies to all carbonyl-carotenoids and polyenes.[44]

Collinearity of the fits of the positions of the S_1 ($2^1A_g^-$) → S_0 ($1^1A_g^-$) transition and the SE spectra measured in ACN suggests that the electronic states associated with both spectral features are similar in their nature. Moreover, it suggests that both transitions are actually associated with the same excited state, and the SE spectrum can originate from stimulated fluorescence induced by the probe light on its long-wavelength tail. However, if this is true, a much more pronounced effect should be observed in the visible range in which the main part of fluorescence is evident. However, the TA spectra clearly show that this is not the case.

In principle, SE is permitted only for optically allowed transitions. Thus, according to this rule, in the measured TA profiles, we should not expect to see any stimulated emission from the S_1 ($2^1A_g^-$) state that is formally forbidden, even though spontaneous emission (i.e., fluorescence) occurs. Therefore, the ICT state as optically allowed is clearly distinguishable from the forbidden S_1 ($2^1A_g^-$) state via the SE process.

If absorption, fluorescence and SE (note the Gaussian curve that traces out the SE spectrum in Figure 10) profiles of C_{33}-peridinin in ACN are compared on a wavenumber scale (Figure 8B), it is clear that (i) all spectra are similar in shape and width; and (ii) SE from the ICT occurs on the long-wavelength edge of the steady-state fluorescence. Therefore, because the emissive transition between the ICT and ground state is allowed, it should be also possible to measure spontaneous ICT → S_0 ($1^1A_g^-$) fluorescence. However, from the present work, it is clear that both the ICT → S_0 ($1^1A_g^-$) and S_1 ($2^1A_g^-$) → S_0 ($1^1A_g^-$) transitions in polar solvent have broad and featureless profiles. Then, very likely the fluorescence lineshapes that can be measured by either steady-state or time-resolved fluorescence spectroscopy will already contain contributions from both transitions.

On the other hand, if the ICT state is associated with an allowed transition, it should be possible to measure the S_0 ($1^1A_g^-$) → ICT steady-state absorption spectrum in polar solvents; however, it is not observed. This means that even though the transition is allowed, the ICT state is not accessible by a vertical transition from the ground state. Very likely, the ICT emission occurs from a molecule that has undergone a substantial nuclear rearrangement compared with its coordinates in the ground state and, therefore, has a large displacement of the excited state (ICT) potential energy surface with respect to ground state. It is known that a large displacement could significantly enhance nonradiative deactivation of the excited state and, in effect, shorten its lifetime.[45] This could be the explanation for the very short lifetime of the ICT state for all of these molecules in polar solvents.

Finally, the effect of the solvent polarity-induced displacement of the potential energy surfaces enhancing nonradiative deactivation may be diminished at low temperature in two independent ways: (i) by reducing the number of vibronic modes that can contribute to nonradiative decay; the clearly discernible enhancement in the vibronic resolution in both the steady-state absorption and fluorescence spectra (Figures 1 and 3) support this view; (ii) as pointed out by Zigmantas et al.,[13] who observed a similar effect of elongation of ICT lifetime for peridinin in frozen protic polar solvents (methanol, ethylene glycol), by lowering the temperature, which may have an effect similar to that of decreasing the solvent polarity, which would then increase the coupling barrier between the S_1 ($2^1A_g^-$) and ICT states.

CONCLUSIONS

(1) Steady-state absorption spectroscopy of peridinin analogues performed at 77 K has revealed features that may be assigned to the symmetry forbidden S_0 ($1^1A_g^-$) → S_1 ($2^1A_g^-$) absorption transition. For peridinin, the assignment of these novel absorption bands is supported by data from previously obtained two-photon excitation spectra.[20]

(2) Time-resolved absorption and fluorescence spectroscopy performed at RT and at 77 K on the peridinin analogues dissolved in solvents having very different polarities revealed more precise lifetimes of the S_1 ($2^1A_g^-$) and ICT states than previously reported. The TA measurements were also expanded into the NIR spectral region.

(3) Time-resolved absorption spectra taken from the analogues dissolved in *n*-hex demonstrated that the yield of spontaneous triplet state formation depends on the length of the π-electron conjugation and, as shown here for the first time, can be very precisely described by the equation $\ln(\Phi_T) = A + B/(2N + 1)$.

(4) Measurements of the SE from the ICT state in the NIR range for the series of peridinin analogues clearly demonstrate, in agreement with previous work,[44] that the ICT state lies in the vicinity of the S_1 ($2^1A_g^-$) state; however, unlike the suggestion from a previous report,[14] the ICT energy level depends on the extent of carotenoid π-electron conjugation.

ASSOCIATED CONTENT

Supporting Information

Transient absorption spectra and time-resolved fluorescence profiles and spectra of peridinin, C_{35}-peridinin, and C_{33}-peridinin taken in *n*-hex, THF, and ACN at RT and in 2-MTHF at 77 K. Global fitting results of the TA data sets, the representative kinetic traces extracted from the TA with the accompanying fits, and the fluorescence decay kinetics extracted from the fluorescence time-resolved profiles of peridinin, C_{35}-peridinin, and C_{33}-peridinin. This material is available free of charge via the Internet at http://pubs.acs.org.

AUTHOR INFORMATION

Corresponding Author

*(D.M.N.) Address: Photosynthetic Antenna Research Center, Washington University in St. Louis, Campus Box 1138, St. Louis, MO 63130, USA. Phone: (314) 935-8483. Fax: (314) 935-4925. (H.A.F.) Phone: (860) 486-2844. Fax: (860) 486-6558.

Notes

The authors declare no competing financial interest.

ACKNOWLEDGMENTS

The steady-state and ultrafast spectroscopic measurements were performed in the Ultrafast Laser facility of the

Photosynthetic Antenna Research Center (PARC), an Energy Frontier Research Center funded by the U.S. Department of Energy, Office of Science, Office of Basic Energy Sciences, under Award No. DE-SC 0001035. Work in H.A.F.'s laboratory was supported by grants from the National Science Foundation (MCB-1243565) and the University of Connecticut Research Foundation. S.K. was supported by a Grant-in-Aid for Science Research on Priority Areas 16073222 from the Ministry of Education, Culture, Sports, Science and Technology, and Matching Fund Subsidy for a Private University, Japan. The authors thank Amy LaFountain and Nikki Magdaong for help with some of the absorption spectroscopic experiments.

REFERENCES

(1) Takaichi, S. Carotenoids and Carotenogenesis in Anoxygenic Photosythetic Bacteria. In *Photochemistry of Carotenoids*; Frank, H. A., et al., Eds.; Kluwer Academic Publishers: Dordrecht/Boston/London, 1999; pp 39−69.

(2) Demmig-Adams, B.; Adams, W. W. I. The Xanthophyll Cycle. In *Carotenoids in Photosynthesis*; Young, A. J., Britton, D., Eds.; Chapman and Hall: London, 1993; p 206.

(3) Christensen, R. L. The Electronic States of Carotenoids. In *Photochemistry of Carotenoids*; Frank, A. J., et al., Eds.; Kluwer Academic Publishers: Dordrecht, Boston, London, 1999; pp 137−159.

(4) Bautista, J. A.; Connors, R. E.; Raju, B. B.; Hiller, R. G.; Sharples, F. P.; Gosztola, D.; Wasielewski, M. R.; Frank, H. A. Excited State Properties of Peridinin: Observation of a Solvent Dependence of the Lowest Excited Singlet State Lifetime and Spectral Behavior Unique among Carotenoids. *J. Phys. Chem. B* **1999**, *103*, 8751−8758.

(5) Frank, H. A.; Bautista, J. A.; Josue, J.; Pendon, Z.; Hiller, R. G.; Sharples, F. P.; Gosztola, D.; Wasielewski, M. R. Effect of the Solvent Environment on the Spectroscopic Properties and Dynamics of the Lowest Excited States of Carotenoids. *J. Phys. Chem. B* **2000**, *104*, 4569−4577.

(6) Wild, D. A.; Winkler, K.; Stalke, S.; Oum, K.; Lenzer, T. Extremely Strong Solvent Dependence of the $S_1 \rightarrow S_0$ Internal Conversion Lifetime of 12′-Apo-B-Caroten-12′-Al. *Phys . Chem. Chem. Phys.* **2006**, *8*, 2499−2505.

(7) Ehlers, F.; Wild, D. A.; Lenzer, T.; Oum, K. Investigation of the $S_1/Ict \rightarrow S_0$ Internal Conversion Lifetime of 4′-Apo-B-Caroten-4′-Al and 8′-Apo-B-Caroten-8′-Al: Dependence on Conjugation Length and Solvent Polarity. *J. Phys. Chem. A* **2007**, *111*, 2257−2265.

(8) Kopczynski, M.; Ehlers, F.; Lenzer, T.; Oum, K. Evidence for an Intramolecular Charge Transfer State in 12′-Apo-B-Caroten-12′-Al and 8′-Apo-B-Caroten-8′-Al: Influence of Solvent Polarity and Temperature. *J. Phys. Chem. A* **2007**, *111*, 5370−5381.

(9) Stalke, S.; Wild, D. A.; Lenzer, T.; Kopczynski, M.; Lohse, P. W.; Oum, K. Solvent-Dependent Ultrafast Internal Conversion Dynamics of *N*′-Apo-Beta-Carotenoic-*N*′-Acids (*N* = 8, 10, 12). *Phys. Chem. Chem. Phys.* **2008**, *10*, 2180−2188.

(10) Chatterjee, N.; Niedzwiedzki, D. M.; Kajikawa, T.; Hasegawa, S.; Katsumura, S.; Frank, H. A. Effect of Π-Electron Conjugation Length on the Solvent-Dependent S_1 Lifetime of Peridinin. *Chem. Phys. Lett.* **2008**, *463*, 219−224.

(11) Zigmantas, D.; Hiller, R. G.; Sharples, F. P.; Frank, H. A.; Sundstrom, V.; Polivka, T. Effect of a Conjugated Carbonyl Group on the Photophysical Properties of Carotenoids. *Phys. Chem. Chem. Phys.* **2004**, *6*, 3009−3016.

(12) Zigmantas, D.; Polivka, T.; Hiller, R. G.; Yartsev, A.; Sundstrom, V. Spectroscopic and Dynamic Properties of the Peridinin Lowest Singlet Excited States. *J. Phys. Chem. A* **2001**, *105*, 10296−10306.

(13) Zigmantas, D.; Hiller, R. G.; Yartsev, A.; Sundstrom, V.; Polivka, T. Dynamics of Excited States of the Carotenoid Peridinin in Polar Solvents: Dependence on Excitation Wavelength, Viscosity, and Temperature. *J. Phys. Chem. B* **2003**, *107*, 5339−5348.

(14) Niedzwiedzki, D. M.; Chatterjee, N.; Enriquez, M. M.; Kajikawa, T.; Hasegawa, S.; Katsumura, S.; Frank, H. A. Spectroscopic Investigation of Peridinin Analogues Having Different Π-Electron Conjugated Chain Lengths: Exploring the Nature of the Intramolecular Charge Transfer State. *J. Phys. Chem. B* **2009**, *113*, 13604−13612.

(15) Vaswani, H. M.; Hsu, C. P.; Head-Gordon, M.; Fleming, G. R. Quantum Chemical Evidence for an Intramolecular Charge-Transfer State in the Carotenoid Peridinin of Peridinin-Chlorophyll-Protein. *J. Phys. Chem. B* **2003**, *107*, 7940−7946.

(16) Van Tassle, A. J.; Prantil, M. A.; Hiller, R. G.; Fleming, G. R. Excited State Structural Dynamics of the Charge Transfer State of Peridinin. *Isr. J. Chem.* **2007**, *47*, 17−24.

(17) Papagiannakis, E.; Larsen, D. S.; van Stokkum, I. H.; Vengris, M.; Hiller, R. G.; van Grondelle, R. Resolving the Excited State Equilibrium of Peridinin in Solution. *Biochemistry* **2004**, *43*, 15303−15309.

(18) Papagiannakis, E.; Vengris, M.; Larsen, D. S.; van Stokkum, I. H.; Hiller, R. G.; van Grondelle, R. Use of Ultrafast Dispersed Pump-Dump-Probe and Pump-Repump-Probe Spectroscopies To Explore the Light-Induced Dynamics of Peridinin in Solution. *J. Phys. Chem. B* **2006**, *110*, 512−521.

(19) Linden, P. A.; Zimmermann, J.; Brixner, T.; Holt, N. E.; Vaswani, H. M.; Hiller, R. G.; Fleming, G. R. Transient Absorption Study of Peridinin and Peridinin-Chlorophyll *a*-Protein after Two-Photon Excitation. *J. Phys. Chem. B* **2004**, *108*, 10340−10345.

(20) Shima, S.; Ilagan, R. P.; Gillespie, N.; Sommer, B. J.; Hiller, R. G.; Sharples, F. P.; Frank, H. A.; Birge, R. R. Two-Photon and Fluorescence Spectroscopy and the Effect of Environment on the Photochemical Properties of Peridinin in Solution and in the Peridinin-Chlorophyll-Protein from *Amphidinium Carterae*. *J. Phys. Chem. A* **2003**, *107*, 8052−8066.

(21) Kajikawa, T.; Hasegawa, S.; Iwashita, T.; Kusumoto, T.; Hashimoto, H.; Niedzwiedzki, D. M.; Frank, H. A.; Katsumura, S. Syntheses of C33-, C35-, and C39-Peridinin and Their Spectral Characteristics. *Org. Lett.* **2009**, *11*, 5006−5009.

(22) Niedzwiedzki, D. M.; Fuciman, M.; Frank, H. A.; Blankenship, R. E. Energy Transfer in an Lh4-Like Light Harvesting Complex from the Aerobic Purple Photosynthetic Bacterium *Roseobacter Denitrificans*. *Biochim. Biophys. Acta, Bioenerg.* **2011**, *1807*, 518−528.

(23) van Stokkum, I. H.; Larsen, D. S.; van Grondelle, R. Global and Target Analysis of Time-Resolved Spectra. *Biochim. Biophys. Acta, Bioenerg.* **2004**, *1657*, 82−104.

(24) Richert, R. Origin of Dispersion in Dipolar Relaxations of Glasses. *Chem. Phys. Lett.* **1993**, *216*, 223−227.

(25) Bublitz, G. U.; Ortiz, R.; Marder, S. R.; Boxer, S. G. Stark Spectroscopy of Donor/Acceptor Substituted Polyenes. *J. Am. Chem. Soc.* **1997**, *119*, 3365−3376.

(26) Dietzek, B.; Chabera, P.; Hanf, R.; Tschierlei, S.; Popp, J.; Pascher, T.; Yartsev, A.; Polivka, T. Optimal Control of Peridinin Excited-State Dynamics. *Chem. Phys.* **2010**, *373*, 129−136.

(27) Bovi, D.; Mezzetti, A.; Vuilleumier, R.; Gaigeot, M. P.; Chazallon, B.; Spezia, R.; Guidoni, L. Environmental Effects on Vibrational Properties of Carotenoids: Experiments and Calculations on Peridinin. *Phys. Chem. Chem. Phys.* **2011**, *13*, 20954−20964.

(28) Ikeyama, T.; Azumi, T. The Fluorescence and the Absorption-Spectra of 1,8-Diphenyl-1,3,5,7-Octatetraene, the Origin of the Transition Moments and the Interpretation of Anomalous Intensity Distribution. *J. Chem. Phys.* **1982**, *76*, 5672−5677.

(29) Henneker, W. H.; Siebrand, W.; Zgierski, M. Z. Quantitative Interpretation of the Absorption and Emission-Spectra of 1,8-Diphenyl-1,3,5,7-Octatetraene. *J. Chem. Phys.* **1983**, *79*, 2495−2496.

(30) Wang, P.; Nakamura, R.; Kanematsu, Y.; Koyama, Y.; Nagae, H.; Nishio, T.; Hashimoto, H.; Zhang, J. P. Low-Lying Singlet States of Carotenoids Having 8−13 Conjugated Double Bonds as Determined by Electronic Absorption Spectroscopy. *Chem. Phys. Lett.* **2005**, *410*, 108−114.

(31) Fujii, R.; Onaka, K.; Kuki, M.; Koyama, Y.; Watanabe, Y. The $2a_g^-$ Energies of All-*Trans*-Neurosporene and Spheroidene as Determined by Fluorescence Spectroscopy. *Chem. Phys. Lett.* **1998**, *288*, 847−853.

(32) Krawczyk, S.; Luchowski, R. Vibronic Structure and Coupling of Higher Excited Electronic States in Carotenoids. *Chem. Phys. Lett.* **2013**, *564*, 83−87.
(33) Premvardhan, L.; Papagiannakis, E.; Hiller, R. G.; van Grondelle, R. The Charge-Transfer Character of the $S_0 \rightarrow S_2$ Transition in the Carotenoid Peridinin Is Revealed by Stark Spectroscopy. *J. Phys. Chem. B* **2005**, *109*, 15589−15597.
(34) Lakowicz, J. R. Solvent and Environmental Effects. In *Principles of Fluorescence Spectroscopy*; Springer: New York, 2006; pp 205−235
(35) Polivka, T.; Zigmantas, D.; Frank, H. A.; Bautista, J. A.; Herek, J. L.; Koyama, Y.; Fujii, R.; Sundstrom, V. Near-Infrared Time-Resolved Study of the S_1 State Dynamics of the Carotenoid Spheroidene. *J. Phys. Chem. B* **2001**, *105*, 1072−1080.
(36) Niedzwiedzki, D. M.; Sullivan, J. O.; Polivka, T.; Birge, R. R.; Frank, H. A. Femtosecond Time-Resolved Transient Absorption Spectroscopy of Xanthophylls. *J. Phys. Chem. B* **2006**, *110*, 22872−22885.
(37) Niedzwiedzki, D. M.; Sandberg, D. J.; Cong, H.; Sandberg, M. N.; Gibson, G. N.; Birge, R. R.; Frank, H. A. Ultrafast Time-Resolved Absorption Spectroscopy of Geometric Isomers of Carotenoids. *Chem. Phys.* **2009**, *357*, 4−16.
(38) Niedzwiedzki, D.; Koscielecki, J. F.; Cong, H.; Sullivan, J. O.; Gibson, G. N.; Birge, R. R.; Frank, H. A. Ultrafast Dynamics and Excited State Spectra of Open-Chain Carotenoids at Room and Low Temperatures. *J. Phys. Chem. B* **2007**, *111*, 5984−5998.
(39) Pendon, Z. D.; Gibson, G. N.; van der Hoef, I.; Lugtenburg, J.; Frank, H. A. Effect of Isomer Geometry on the Steady-State Absorption Spectra and Femtosecond Time-Resolved Dynamics of Carotenoids. *J. Phys. Chem. B* **2005**, *109*, 21172−21179.
(40) Cong, H.; Niedzwiedzki, D. M.; Gibson, G. N.; Frank, H. A. Ultrafast Time-Resolved Spectroscopy of Xanthophylls at Low Temperature. *J. Phys. Chem. B* **2008**, *112*, 3558−3567.
(41) Kaligotla, S.; Doyle, S.; Niedzwiedzki, D. M.; Hasegawa, S.; Kajikawa, T.; Katsumura, S.; Frank, H. A. Triplet State Spectra and Dynamics of Peridinin Analogs Having Different Extents of π-Electron Conjugation. *Photosynth. Res.* **2010**, *103*, 167−174.
(42) Fuciman, M.; Enriquez, M. M.; Kaligotla, S.; Niedzwiedzki, D. M.; Kajikawa, T.; Aoki, K.; Katsumura, S.; Frank, H. A. Singlet and Triplet State Spectra and Dynamics of Structurally Modified Peridinins. *J. Phys. Chem. B* **2011**, *115*, 4436−4445.
(43) Hashimoto, H.; Koyama, Y.; Hirata, Y.; Mataga, N. S_1 and T_1 Species of B-Carotene Generated by Direct Photoexcitation from the All-*Trans*, 9-*Cis*, 13-*Cis*, and 15-*Cis* Isomers as Revealed by Picosecond Transient Absorption and Transient Raman Spectroscopies. *J. Phys. Chem.* **1991**, *95*, 3072−3076.
(44) Enriquez, M. M.; Fuciman, M.; LaFountain, A. M.; Wagner, N. L.; Birge, R. R.; Frank, H. A. The Intramolecular Charge Transfer State in Carbonyl-Containing Polyenes and Carotenoids. *J. Phys. Chem. B* **2010**, *114*, 12416−12426.
(45) Birks, J. B. *Photophysics of Aromatic Molecules*; John Wiley & Sons Ltd.: London, 1970; p 704.